Chinese Chemical Letters 34 (2023) 107600

Contents lists available at ScienceDirect

Chinese Chemical Letters

journal homepage: www.elsevier.com/locate/cclet

Recent advances for Zn-gas batteries beyond Zn-air/oxygen battery

Rong Zhang[a], Zhuoxi Wu[a], Zhaodong Huang[a], Ying Guo[a], Shaoce Zhang[a], Yuwei Zhao[a], Chunyi Zhi[a,b,*]

[a] Department of Materials Science and Engineering, City University of Hong Kong, Hong Kong 999077, China
[b] Centre for Functional Photonics, City University of Hong Kong, Hong Kong 999077, China

ARTICLE INFO

Article history:
Received 5 January 2022
Revised 3 March 2022
Accepted 8 June 2022
Available online 13 June 2022

Keywords:
Zn-CO_2 battery
Zn-N_2 battery
Zn-NO battery
Electrocatalysts
Value-added chemicals

ABSTRACT

Zn-gas batteries have attracted great attention in the area of energy conversion and storage owing to their high theoretical energy density in the past decades. In addition to the most widely researched Zn-air/oxygen battery, other novel Zn-gas batteries such as Zn-CO_2, Zn-N_2 and Zn-NO batteries as "killing two birds with one stone" strategy have emerged to provide energy power and upgrade the pollutant/useless gases simultaneously. This technology becomes more appealing as a low-cost and controllable method to produce value-added chemicals and fuels (such as CO, $HCOO^-$, CH_4, NH_3) at the cathode driven by surplus electricity. However, there is an absence of a guide for the selection of catalyst and the construction of energy system. Herein, we overview recent achievements in typical Zn-gas batteries beyond Zn-air/oxygen, mainly including Zn-CO_2, Zn-N_2 and Zn-NO batteries. The energy storage mechanism of these novel Zn-gas batteries has been clearly elaborated. Then, the produced value-added chemicals and the design of cathodic catalyst materials are summarized. Lastly, the remaining challenges and possible directions of Zn-gas batteries, such as highly reduced products, high yield rate and remarkable battery performance, in the future are discussed.

1. Introduction

The increasing demand for energy supply and rapid consumption of fossil fuels cause concerns for sustainable human society, accelerating the exploration of advanced energy conversion and storage technique [1–3]. As a kind of ideal energy storage device, batteries can store the energy generated by intermittent clean energy and are helpful in shaving the peak of the power grid [4–6]. Zinc-based batteries (ZBs), with merits of abundance, safety, chemical stability, low cost, and environmental friendliness, are promising choice for large-scale energy storage [7–9]. Among the ZBs, zinc-air batteries (ZABs) are the most practically viable battery systems owing to a high specific capability, a high theoretical energy, excellent safety and good corrosion resistance [10–13]. The cycle of ZABs generally involves oxygen reduction reaction (ORR) and oxygen evolution reaction (OER) processes at the cathode. During the discharge process, O_2 is adsorbed on the surface of the solid catalyst. Then O=O bond is activated and broken to generate the intermediates, which react with Zn^{2+} to produce discharge species (such as $Zn(OH)_2$ or ZnO_2). However, in addition to O_2, there are many other gases, such as CO_2, N_2 and NO, as important compositions in ambient air and they can be electrochemically reduced to various value-added chemicals under certain conditions. Employing these gases as the cathode, the novel Zn-gas batteries have been recently reported with unique advantages of producing value-added chemicals from these pollutant/useless gases compared to ZABs [14,15].

With the rapid development of human society, the concentration of global CO_2 from fossil fuel combustion is increasing rapidly and emitted to atmosphere, causing serious anthropogenic climate changes [16–24]. Another major environmental gas contamination, NO, which comes from the industrial processes (*e.g.*, coal-fired power plants and motor vehicles), would causes serious environmental and ecological issues, such as acid rain, ozone depletion, and haze, posing potential risks to human health [25,26]. N_2 is the most abundant resource in the air, and it is of great significance to produce NH_3 by the reduction of N_2. The removal and upgrading of these gases are thus highly attractive for economic and environmental issues [4,27–30]. Electrochemical method is employed to convert these gases to valuable chemicals [31,32]. For example, using efficient catalysts, CO_2 can be reduced into various fuels and chemicals (such as CO, HCOOH, CH_4, alcohols) [33–35] while NO and N_2 can be selectively reduced to NH_3 [36–39], which is a vital building block for both agricultural and industrial products, as well as a promising energy carrier for hydrogen [40,41]. The utilization

* Corresponding author.
E-mail address: cy.zhi@cityu.edu.hk (C. Zhi).

https://doi.org/10.1016/j.cclet.2022.06.023
1001-8417/

of these gases with Zn anode to develop novel Zn-CO_2/N_2/NO batteries offers a promising "clean" strategy to reduce fossil fuel consumption and consequently, purifying the environment. Moreover, value-added chemicals or fuels can be generated from the battery systems. It is more attractive to develop Zn-CO_2 batteries as potential energy conversion and chemicals production devices for scientific exploration and future immigration to Mars since the air there contains 95% of CO_2 [42].

Here, the recent development of Zn-gas batteries beyond ZABs, including battery reaction mechanisms and newly developed catalyst cathodes, are summarized. We aim to shed light on how these gases, such as CO_2/N_2/NO, works for electrochemical conversion in Zn-gas batteries. The current challenges and future directions for the development of Zn-gas batteries are also discussed. We hope to motivate more studies on Zn-gas battery systems to better promote these gases conversion efficiency in energy conversion and storage devices.

2. Zn-CO_2 batteries

2.1. Mechanisms

Different from Li/Na-CO_2 batteries under water-free and oxygen-free conditions, Zn-CO_2 batteries with environmental benignity can directly work in aqueous electrolyte due to the relatively low activity of Zn metal [42]. The aqueous electrolyte with abundant protons provides a proton coupled electron transfer pathway to convert CO_2 into different carbon-containing products. This feature is also different from Li/Na-CO_2 batteries, where CO_2 is cycled during discharging and charging processes. Although the energy density of aqueous Zn-CO_2 batteries is theoretically lower than that for Li/Na-CO_2 batteries, the aqueous Zn-CO_2 batteries possesses a unique merit for low-cost Zn anode and production of abundant value-added chemicals. From the viewpoint of thermodynamics, Zn-CO_2 batteries for various chemicals production can be developed based on the Zn/ZnO standard reduction potential (1.22 V *vs.* standard hydrogen electrode) in alkaline electrolytes [20,43,44].

Currently, three Zn-CO_2 batteries for CO, HCOOH and CH_4 production have been developed. Generally, the Zn-CO_2 batteries are conducted using a H-type configuration separated by a bipolar membrane. One chamber is composed with Zn anode and basic aqueous electrolyte while the other chamber consists of neutral aqueous electrolyte (typically $KHCO_3$ solution) and catalyst cathode with high selectivity and activity. For CO_2-to-CO conversion in a Zn-CO_2 battery, the reaction mechanism can be written as follows [45,46]:

Discharging process:

$$\text{Cathode: } CO_2 + H_2O + 2e^- \rightarrow CO + 2OH^-$$

$$\text{Anode: } Zn + 2OH^- \rightarrow ZnO + H_2O + 2e^- \text{ (1 mol/L KOH)}$$

$$Zn + 4OH^- \rightarrow Zn(OH)_4^{2-} + 2e^- \text{ (6 mol/L KOH)}$$

Charging process:

$$\text{Cathode: } 4OH^- \rightarrow O_2 + 2H_2O + 4e^-$$

$$\text{Anode: } ZnO + H_2O + 2e^- \rightarrow Zn + 2OH^- \text{ (1 mol/L KOH)}$$

$$Zn(OH)_4^{2-} + 2e^- \rightarrow Zn + 4OH^- \text{ (6 mol/L KOH)}$$

Overall reaction: $CO_2 \rightarrow CO + O_2$

In terms of Zn-CO_2 battery for HCOOH production, the reactions during charging process are various. HCOOH is a kind of liquid product with high solubility in water and it is easy to be oxidized [47]. Format oxidation reaction (FOR) and OER may occur simultaneously during charging process. There are three reported mechanisms for Zn-CO_2 battery for HCOOH production. The first mechanism is similar to the that for CO generation, where OER occurs during charging process at the cathode [48–50]. The second is that OER and FOR occur simultaneously during charging process [51]. The last one is that only FOR occurs at the cathode. For instance, Xie *et al.* reported a reversible aqueous Zn-CO_2 battery based on $Zn + CO_2 + 2H^+ + 2OH^- = ZnO + HCOOH + H_2O$ [52]. In this battery, the OER is significantly suppressed due to the large overpotential of OER over porous Pd catalyst and the reversible conversion between CO_2 and HCOOH is achieved. Compared with the dual reactions (CO_2 reduction reaction (CRR) and OER) on the cathodes, the resulting reversible aqueous Zn-CO_2 battery shows a much lower charge voltage and a higher energy efficiency of 81.2%.

However, the reported Zn-CO_2 battery for CH_4 generation is a type of primary battery [53,54]. According to the current report, a CNT hollow fiber and a Zn wire were paired within a custom-designed cell filled by 1-ethyl-3-methylimidazolium tetrafluoroborate [EMIM][BF_4] to form a single-compartment Zn-CO_2 flow battery [53]. CO_2 react with hydrogen provided by [EMIM][BF_4] to produce CH_4 at the cathode during discharging process. Hydrogen at the C_2 position of the imidazolium ring is acidic and proton source which may react with basic $Zn(OH)_2$ to form water and N-heterocyclic carbene complex. This type of Zn-CO_2 battery is a primary battery but it is renewable as the oxidized Zn anode is electrochemically reducible to elemental Zn^0.

2.2. Catalyst cathodes for Zn-CO_2 batteries

Efficient catalyst materials are crucial to accelerate the CO_2 reduction reaction kinetics and lower the overpotential, enabling the Zn-CO_2 battery systems to discharge more spontaneously [55]. Meantime, aqueous CO_2 reduction suffers from competitive H_2 evolution reaction (HER) [56]. Furthermore, the OER usually occurs at the cathode during the charge process of aqueous Zn-CO_2 batteries. Therefore, a highly selective and active bifunctional catalyst for CRR and OER with suppressed HER activity is ideal to realize a high-performance Zn-CO_2 battery. Based on several types of catalysts used in Zn-CO_2 battery, we compared their activity, selectivity, price, and stability.

2.2.1. Catalyst cathodes for Zn-CO_2 batteries for CO production

Noble metals: Noble metal Au has attracted considerable attentions owing to the remarkable activity for CRR to CO because it has a strong adsorption ability for key intermediate (*e.g.*, *CO, *COOH) [57]. Employing coralloid Au as cathodic material, Sun *et al.* developed an aqueous Zn-CO_2 battery with a power density of 0.7 mW/cm^2, 68 h cyclability, and a 63% FE for CO production [58]. Considering that Ir is the most active metal for OER during charging process, Yao *et al.* fabricated an Ir@Au bimetal catalyst (Fig. 1a) material as bifunctional cathode to promote the battery discharge output and energy efficiency [59]. During constant current discharge/charge tests, the battery shows a discharging voltage of +0.74 V at 0.01 mA with an energy density of 610 Wh/kg. The charging voltage of the battery is 2.25 V at 0.01 mA, much smaller than that using Au catalyst as cathode (Figs. 1b and c). The assembled Zn-CO_2 battery for CO synthesis shows 67% and 90% Faradaic efficiency (FE) at a discharge current of 0.5 mA (2.8 mA/cm^2) and 1.5 mA (8.3 mA/cm^2) (Fig. 1d), respectively. However, the stability is unsatisfying and the galvanostatic discharge-charge cycling at 0.9

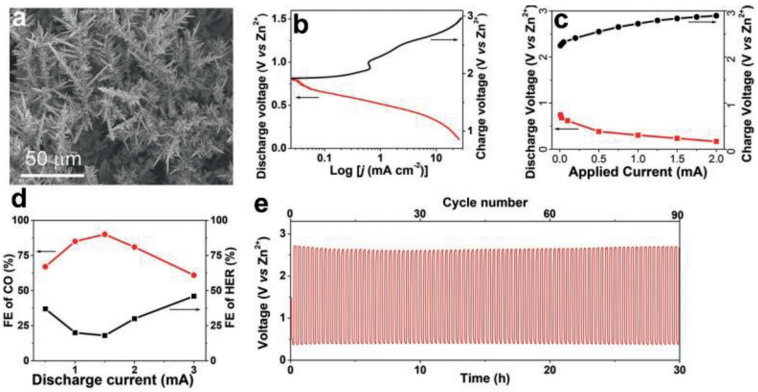

Fig. 1. (a) Scanning electronic microscope (SEM) image of Ir@Au. (b) Discharge and charge polarization curves. (c) Discharge and charge voltage profiles. (d) CO FE and H_2 FE during discharge process. (e) Long-term discharge-charge cycling curves at 5 mA/cm^2 for 90 cycles. Copied with permission [59]. Copyright 2018, Wiley-VCH.

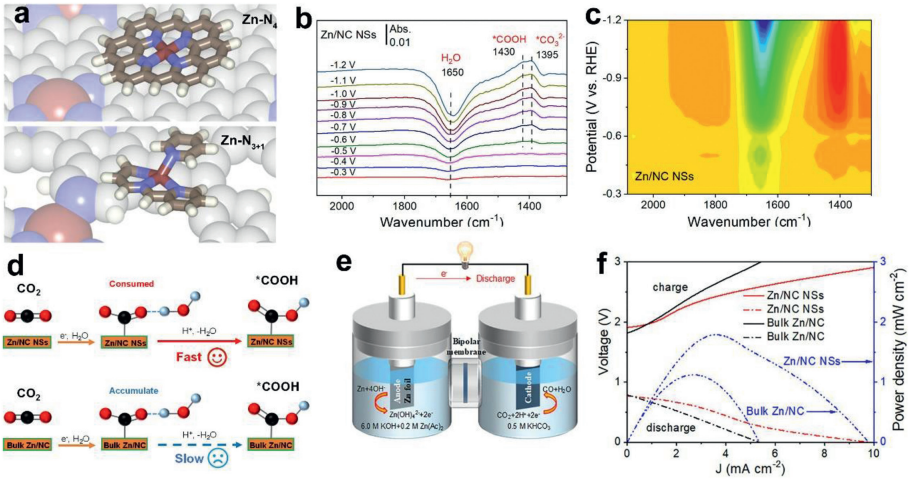

Fig. 2. (a) Models of Zn-N_4 and Zn-N_{3+1} SACs. (b) *In situ* ATR-FTIR spectra during CRR and (c) the corresponding contour map on Zn/NC NSs. (d) Proposed reaction mechanisms. (e) Illustration of a designed Zn-CO_2 battery. (f) Charge-discharge curves and power densities of a Zn-CO_2 battery. Copied with permission [62]. Copyright 2021, Wiley-VCH.

mA only maintained 30 h for 90 cycles. In addition, the high cost and inferior activity of noble metal catalysts hinder their large-scale applications (Fig. 1e). Hence, it is important to develop cost-efficient alternative catalysts with more stable structure, higher activity and selectivity for Zn-CO_2 batteries.

Transition metal-based single-atom catalysts: Compared to noble metals, the cost-effective transition metal based single-atom catalysts (SACs) with maximized utilization of metal atoms and attractive activity have received considerate interests in electrocatalytic CRR [60]. Zn, Co, Mn, Ni, Fe and Cu SACs have been reported as catalyst cathodes for Zn-CO_2 batteries. A series of hierarchical cross-linked nanostructured carbon aerogels with M-N_4 sites (CA/N-M, M = Ni, Fe, Co, Mn, and Cu) were reported for CRR and Zn-CO_2 battery [61]. The CRR activity of CA/N-M aerogels exhibits a negative correlation with different metals, following order of CA/N-Cu < CA/N-Mn < CA/N-Co < CA/N-Fe < CA/N-Ni.

In order to further enhance the battery performance, these SACs are well designed and explored to achieve superior catalytic activity for CRR and/or OER. For instance, different from many reported plane SACs, Hou *et al.* prepared atomically dispersed zinc(I) anchored on N-doped carbon nanosheets (Zn/NC NSs) with a twisted M-N_4 configuration (Fig. 2a) for Zn-CO_2 battery [62]. CRR process involves two key intermediates (*COOH and *CO) *via* the protonation process. While the plane symmetrical structure of the M-N_4 moieties shows a high reaction free energy for water dissociation step, the Zn/NC NSs with structural distortion can enhance the water dissociation process and promote protons transfer, thereby accelerating the catalytic kinetics. *In-situ* attenuated total reflectance infrared absorption spectroscopy (ATR-FTIR) and theoretical calculations are employed to prove that twisted M-N_4 structure accelerates the CO_2 activation and protonation in the rate-determining step of *CO_2 to *COOH on the rationally engineered proton-feeding centers, promoting the proton-coupled CRR kinetics and boosting the overall catalytic performance (Figs. 2b-d). A rechargeable Zn-CO_2 battery based on the Zn/NC NS cathode delivers an open-circuit potential of +0.769 V and a power density of 1.8 mW/cm^2 (Figs. 2e and f). A high FE CO of 95% is achieved at 1.5 mA/cm^2 during discharging process and the continuous discharge-charge cycles at 1.5 mA/cm^2 show a good stable stability for 100 cycles. However, Wang *et al.* reported that M-N_4 is not the active centers in Fe SAC [63]. They fabricated a single-atom Fe-N_4 sites with intrinsic carbon defects and found that the intrinsic defect was the active sites for CRR, leading to a reduced energy barrier for CRR and suppressed the HER activity over the catalyst. A rechargeable Zn-CO_2 battery exhibits a high CO FE of 86.5% at 5 mA/cm^2 and remarkable stability for 150 cycles (over 50 h).

It is well known that changing the local electronic and geometric configurations of center metal on SAC would affect CO_2 activation and intermediate absorption/adsorption ability, which further affect the CRR catalytic performance [64]. The coordinatively unsaturated SACs tends to show higher catalytic activity according to the reports. Hou's group reported an isolated Fe atoms on N-

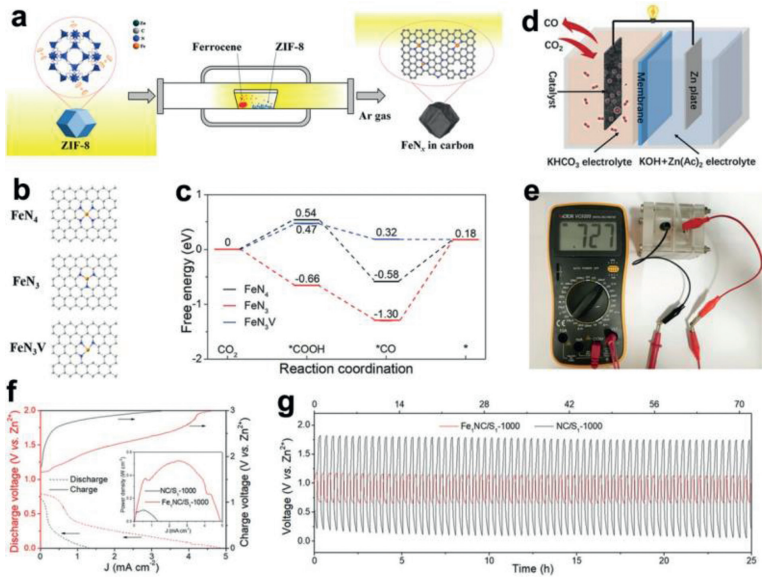

Fig. 3. (a) Schematic illustration of synthetic procedure for gas diffusion strategy. (b) Top view of the optimized atomic structures. (c) Calculated free-energy diagrams for CRR. (d) Schematic configuration and (e) open-circuit potential of Zn-CO_2 battery. (f) Polarization and power density plots. (g) Galvanostatic discharge-charge cycling plots at 0.5 mA/cm^2 for 72 cycles. Copied with permission [65]. Copyright 2020, Wiley-VCH.

doped porous carbon polyhedrons (Fe_1NC) by a gas diffusion strategy (Fig. 3a) [65]. Owing to the presence of highly catalytic active isolated Fe-N_3 sites and graphitic N species, the Fe_1NC catalyst exhibited remarkably catalytic activity for CO generation *via* CRR (Figs. 3b and c). It is attributed to the enhanced accessibility and intrinsic activity of active centers due to the increased electrochemical surface area and the redistribution of doped N species. Zn-CO_2 battery with Fe_1NC catalyst as cathode materials shows a power density up to 526 mW/cm^2 and an open-circuit potential of 0.727 V, which was close to a theoretical electromotive force of +0.707 V (Figs. 3d-f). Moreover, a superior rechargeable stability was demonstrated with a stable narrow discharge-recharge voltage gap of about 0.5 V over consecutive 72 cycles for 25 h at 0.5 mA/cm^2 (Fig. 3g). The subsequent research also suggests that M-N_2 centers are more active than M-N_4. For instance, Feng *et al.* coordinatively unsaturated single-atom copper coordinated with nitrogen sites anchored into graphene matrix (Cu-N_2/GN) as a highly efficient CRR electrocatalyst [45]. Compared to Cu-N_4 structure, such Cu-N_2 site shows more optimized reaction free energy for CO_2 adsorption and more rapid electron transfer from Cu-N_2 sites to absorbed CO_2, thereby enhancing the *COOH generation and CRR performance (Figs. 4a-d). A rechargeable Zn-CO_2 battery with Cu-N_2/GN as cathode shows a peak power density of 0.6 mA/cm^2 at 1.06 mA/cm^2 and the charge process of battery can be driven by natural solar energy (Figs. 4e and f). A CO FE of 64% was achieved at the discharge current density of 1.4 mA/cm^2 (Fig. 4g) and the Zn-CO_2 battery can be recycled at a constant current density of 1.0 mA/cm^2 for over 40 h (Fig. 4h).

While inheriting the exceptional merits of single atom catalysts, diatomic site catalysts (DASCs) utilizing two adjacent atomic metal species for their complementary functionalities and synergistic actions are also reported for Zn-CO_2 battery [66,67]. Jiang *et al.* prepared a novel Fe_1-Ni_1-N-C DASCs with neighboring Fe and Ni single-atom pairs decorated on nitrogen-doped carbon support (Fig. 5a) [67]. Due to synergism of neighboring Fe and Ni single-atom pairs, Fe_1-Ni_1-N-C shows greatly enhanced electrocatalytic activity for CRR, much superior to Fe_1-N-C and Ni_1-N-C (Figs. 5b and c). Zn-CO_2 battery with Fe_1-Ni_1-N-C cathodic material exhibits a high CO FE of 93.4% at 1 mA discharging current and the CO FE can be well maintained over 15 h under consecutive discharge-charge processes (Figs. 5d and e). Theoretical calculations reveal that single-atom Ni can activate the adjacent Fe atoms in Fe_1-Ni_1-N-C through non-bonding interaction, greatly enhancing the generation of COOH* intermediate and thereby promoting CRR performance (Figs. 5f-h). Focusing on both CRR and OER at the cathode, another bifunctional nickel-iron DASC was also reported. The orbital coupling between the catalytic iron center and the adjacent nickel atom leads to alteration in orbital energy level, unique electronic states, higher oxidation state of iron, and weakened binding strength to the reaction intermediates, thus boosted CRR and OER performance.

Carbon-based materials: Compared to SACs, carbon materials are mainly composed of carbon and even can be made directly out of biomass, they are obviously "sustainable" [68,69]. With the unique nanostructure, excellent conductivity, chemical stability and adsorption properties, carbon materials are also explored in the field of Zn-CO_2 battery for CO production [70–73]. Liu *et al.* fabricated nitrogen-doped ordered mesoporous carbon (NOMC) as a bifunctional metal-free electrocatalyst for CRR and OER (Fig. 6a) [70]. The ordered mesoporous structures and abundant N-dopants of NOMC provides a number of active sites, endowing NOMC with excellent catalytic performance and outstanding stability. Zn-CO_2 battery using NOMC with a stable open-circuit voltage of 0.9 V yields a power density of 0.71 mW/cm^2 at a current density of 3.0 mA/cm^2, a good cyclability of 300 cycles, and excellent energy efficiency of 52.8% at 1.0 mA/cm^2. To simply the preparation process and increase the porosity, a cedar biomass-derived three-dimensional (3D) N-doped graphitized carbon is developed and further applied in a Zn-CO_2 battery [71]. The assembled Zn-CO_2 battery with a stable open circuit voltage of 0.79 V shows a peak power density of 0.51 mW/cm^2 at 2.14 mA/cm^2 and a maximum CO FE of 80.4% at 2.56 mA/cm^2 (Figs. 6b-d). Wang *et al.* proposed a carbon matrix containing silicon, nitrogen, and fluorine as a bifunctional catalyst cathode for a solid-state Zn-CO_2 electrochemical cell and the cell can be powered by solar [72]. They showed an interesting artificial leaf system. Electricity generated by the photovoltaic cell can be stored in the artificial leaf during the charging process. The Zn-CO_2 battery shows a FE of 88% for CO generation at 0.1 mA with a discharge voltage of 0.47 V. A solar-to-CO efficiency of 15.2% was achieved with pure CO_2 supply.

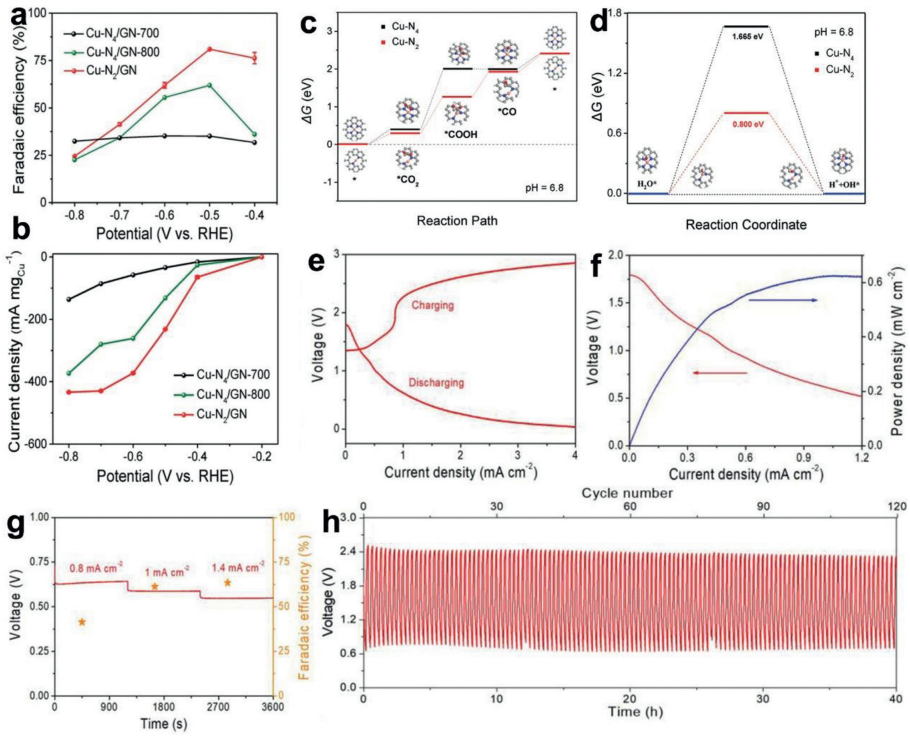

Fig. 4. (a) CO FE for each catalyst. (b) Mass specific partial current densities for CO production. Free energy profile for (c) CRR and (d) water dissociation. (e) Charge-discharge polarization curves and (f) power density curves of Zn-CO_2 battery using Cu-N_2/GN. (g) Galvanostatic discharge curves and corresponding CO FE. (h) Galvanostatic charge-discharge cycling curves at 1 mA/cm^2. Copied with permission [45]. Copyright 2020, Wiley-VCH.

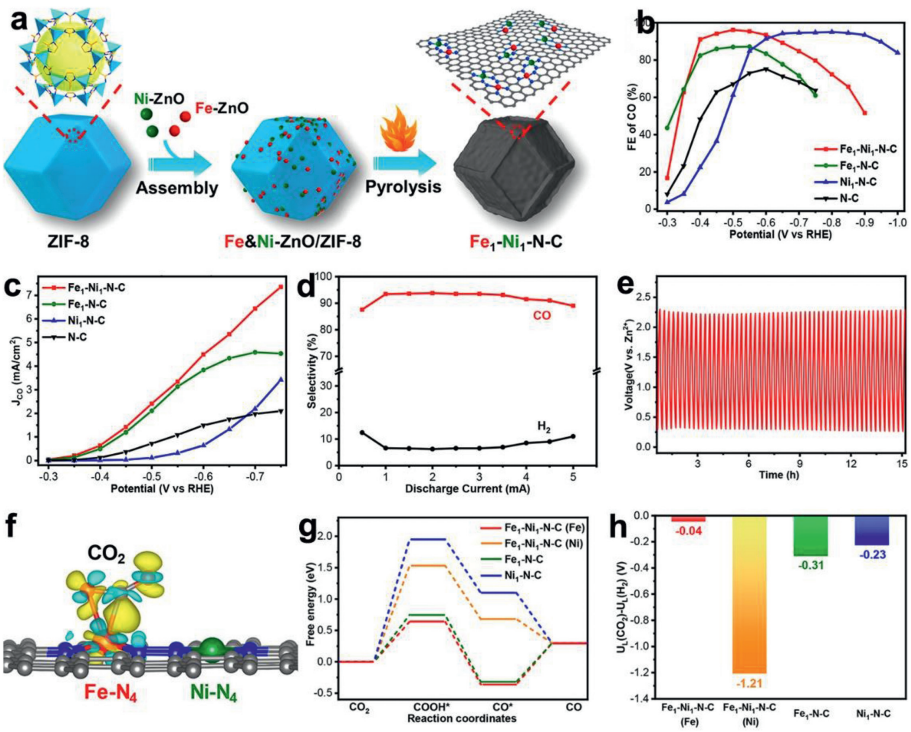

Fig. 5. (a) Schematic illustration for syntheses of Fe_1-Ni_1-N-C. (b) FEs of CO for each catalyst. (c) The partial current density for CO. (d) CO FE and H_2 FE for Zn-CO_2 battery using e_1-Ni_1-N-C catalyst. (e) Discharge-charge stability test at 1.1 mA. (f) Electron density difference analysis of CO_2 absorbed on catalyst. (g) Free energy diagrams of CRR. (h) The $U_L(CO_2)$ – $U_L(H_2)$ values of Fe and Ni sites. Copied with permission [67]. Copyright 2021, American Chemical Society.

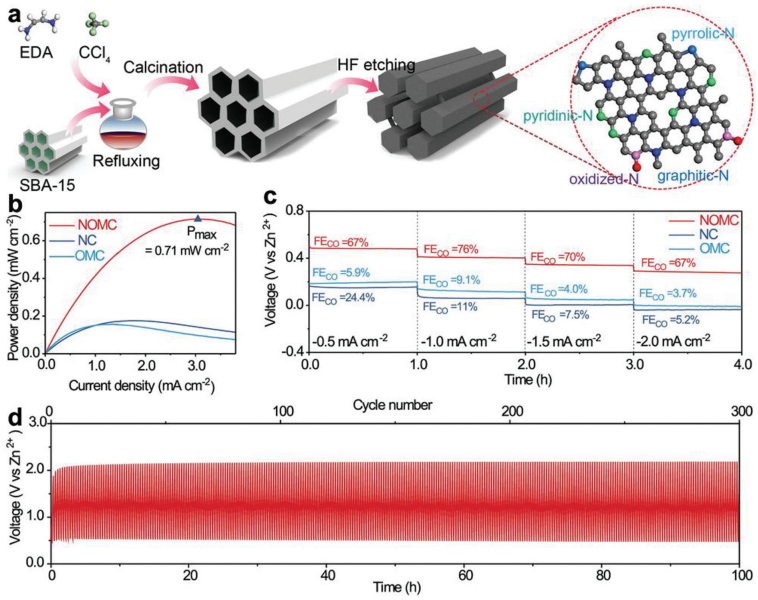

Fig. 6. (a) Schematic illustration of NOMC preparation. (b) Power density curves of assembled Zn-CO_2 battery. (c) Galvanostatic discharge curves at different current densities and the corresponding CO FE. (d) Galvanostatic discharge-charge cycling curves at 1.0 mA/cm^2. Copied with permission [70]. Copyright 2021, Wiley-VCH.

Transition metal compounds: In addition to the SACs and carbon-based materials, transition metal-based compounds such as selenide, phosphide, oxide and hydroxide are also reported for Zn-CO_2 batteries for CO production but most of their catalytic performance are inferior compared to noble metal catalyst and SACs [74–76]. The preparation conditions of these compounds are much milder compared to SAC and the surface configuration can be flexibly tuned by the composition and nanostructure. For example, Hu *et al.* reported a bimetallic $CuInSe_2$ with Se vacancies (V-$CuInSe_2$) (Figs. 7a-c) for Zn-CO_2 battery with superior activity because of the interaction of In and Cu orbitals [74]. The free energy for adsorbed intermediates can be moderately tuned over $CuInSe_2$, thereby delivering enhanced CRR activity compared to monometallic selenides (Figs. 7d and e). Meantime the HER is significantly suppressed due to a lattice reconstruction, which occurs after protons are adsorbed on the catalyst surface. Moreover, the Se vacancies have been proved to enhance the electrons delocalization, which further promotes the CRR activity. The V-$CuInSe_2$ was then applied as the cathode in an aqueous rechargeable Zn-CO_2 battery. The battery exhibits a stable discharge voltage at 0.5 mA/cm^2 for at least 40 h (Fig. 7f). In addition, this rechargeable Zn-CO_2 battery shows a charge and discharge voltages of ~2.4 V and ~0.55 V, respectively, with a superior stability for 70 h (Figs. 7g and h).

Hybrids: Some SACs based hybrids are reported with higher the capability of adsorbing CO_2 and dissociating water for CRR. For instance, a porous Ni-N-C catalyst containing atomically dispersed Ni-N_4 sites and nanostructured zirconium oxide (ZrO_2@Ni-NC) was synthesized (Fig. 8a) [77]. The as-prepared ZrO_2@Ni-NC exhibits an onset potential of −0.3 V, a peak CO FE of 98.6%±1.3% as well as a low Tafel slope of 71.7 mV/dec for CRR in a three-electrode setup. The isolated Ni-N_4 species is identified as real active centers and the ZrO_2 is proved to accelerate the formation rate of *COOH intermediate (Figs. 8b and c). The corresponding Zn-CO_2 battery shows an onset voltage of 0.727 V during discharge process (Fig. 8d). The cathode ZrO_2@Ni-NC shows a wide CO FE range of >90% and the maximum CO FE of 94.3% at 4.0 mA (Fig. 8e). The galvanostatic discharge-charge cycling test of ZrO_2@Ni-NC-based Zn-CO_2 battery demonstrates that the voltage can be well maintained for 33 h (Fig. 8f). An ultrathin p-n type Cu_2O/CuCoCr-layered double hydroxide (U-Cu_2O/CuCoCrLDH) heterojunction was employed for a photo-assisted aqueous Zn-CO_2 batteries. The particular heterojunction is beneficial to the separation of photogenerated electrons and holes under illumination. The aqueous Zn-CO_2 batteries with U-Cu_2O/CuCoCrLDH cathode attained 2.48 and 0.59 V for charge and discharge process, respectively, without assistance of light. However, with photo assistance, the charge voltage decreased to 2.07 V and the discharge voltage increased to 1.22 V. The round-trip efficiency of the battery is improved from 23.79% to 58.94%. CO is identified as the major product along with the formation of CH_4. Other composite catalysts such as Cu_3P decorated on C and Ni nanoparticles decorated on CNTs are also applied to Zn-CO_2 reduction with superior performance [78].

2.2.2. Catalyst cathodes for Zn-CO_2 batteries for $HCOO^-$ production

Metal catalysts: Due to the unique property of H adsorption/absorption, noble metal Pd is used to enable the CRR to $HCOO^-$ with the smallest overpotentials [79]. By tuning the catalyst particle size, and shape, Pd-based catalysts can be enhanced to achieve high FE and partial currents. Xie *et al.* first reported a 3D porous Pd nanosheet with rich edge and pore structure for reversible aqueous Zn-CO_2 battery [52]. Formic acid was proven to be major discharge products with high FE of over 90% at a current density of 15 mA/cm^2. The reaction mechanism of formic acid was $Zn + CO_2 + 2H^+ + 2OH^- \leftrightarrow ZnO + HCOOH + H_2O$. The battery remained durable over 100 cycles after 10-h operation. Non-noble metals have also been reported for HCOOH production using a Zn-CO_2 battery considering the low cost for applications. Zheng *et al.* surface-lithium-doped tin (s-SnLi) catalyst equipped Zn-CO_2 batteries with the highest power densities of 1.24 mW/cm^2 at 8.8 mA/cm^2 [48]. The s-SnLi cathode exhibited a high discharge capacity of 790 mAh/g at 2.0 mA/cm^2, close to the theoretical capacity of Zn (825 mAh/g). However, the reaction during charging process is unclear. Bi is also an active element for CO_2 reduction to HCOOH [35,80]. Therefore, Bi nanoparticles embedded in pyrrolic-N-dominated doped carbon nanosheets (PNCB) was also used as a catalyst anode for Zn-CO_2 batteries with an open circuit potential of ~1.1 V and power density of 1.43 mW/cm^2 at 2 mA/cm^2 [51]. The FEs for formate gradually increased to 80% at 8 mA/cm^2 during discharge process. OER and FOR happened simultaneously during charging process.

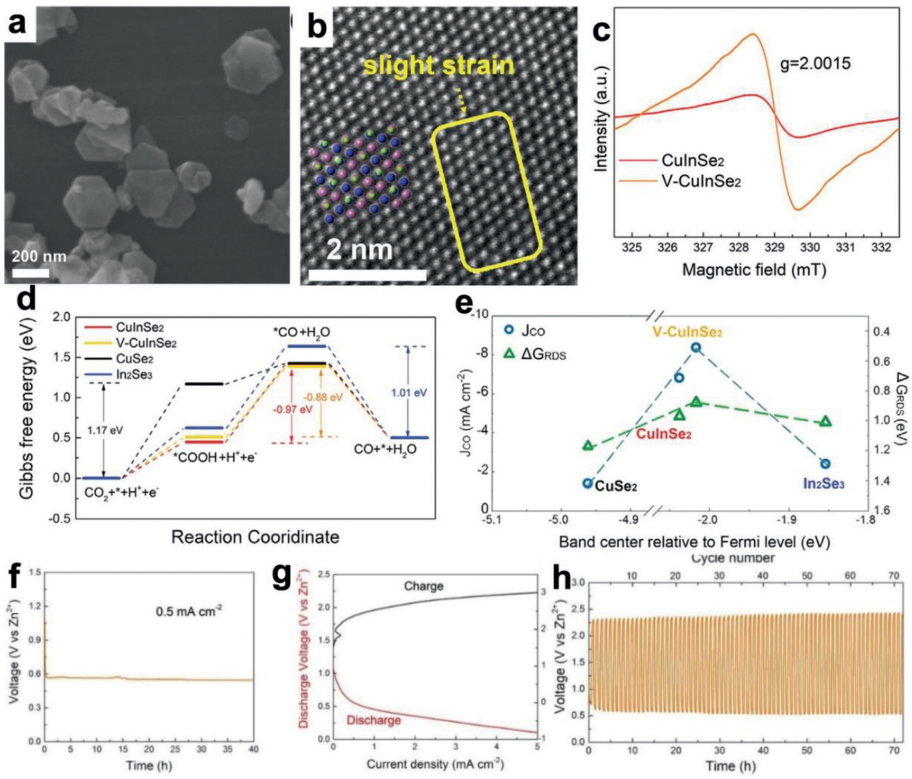

Fig. 7. (a) SEM and (b) atomic-resolution high-angle annular dark-field STEM image of $CuInSe_2$. (c) ESR spectra of $CuInSe_2$ and V-$CuInSe_2$. (d) Gibbs free energy changes of CRR route. (e) Current density for CO generation at −0.7 V *vs.* RHE and the Gibbs free energy for rate-determining step (ΔG_{RDS}) for CRR relative to the band center position. (f) Long-term discharge stability at the current density of 0.5 mA/cm^2. (g) Discharge and charge profiles. (h) Discharge-charge cycling curves at 0.5 mA/cm^2 of Zn-CO_2 cell using V-$CuInSe_2$ as the cathode. Copied with permission [74]. Copyright 2021, Wiley-VCH.

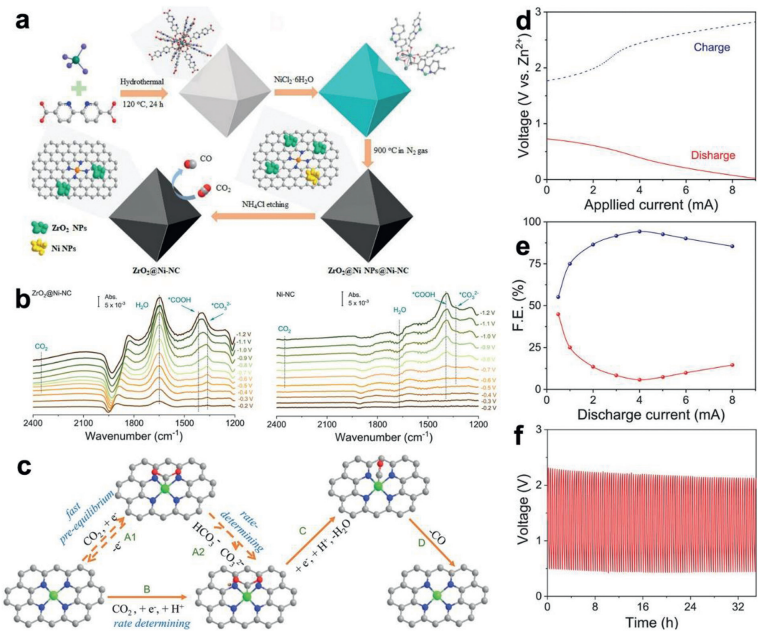

Fig. 8. (a) Schematic illustration of the synthesis of ZrO_2@Ni-NC. *In situ* ATR-FTIR spectra of ZrO_2@Ni-NC (left) and Ni-NC (right). (c) Schematic illustration of the CRR reaction mechanisms of ZrO_2@Ni-NC and Ni-NC. (d) Charge and discharge curves of ZrO_2@Ni-NC. (e) CO and H_2 FE of ZrO_2@Ni-NC at corresponding discharge currents. (f) Galvanostatic discharge-charge cycling curve of ZrO_2@Ni-NC equipped Zn-CO_2 battery at 1.0 mA/cm^2. Copied with permission [77]. Copyright 2021, Wiley-VCH.

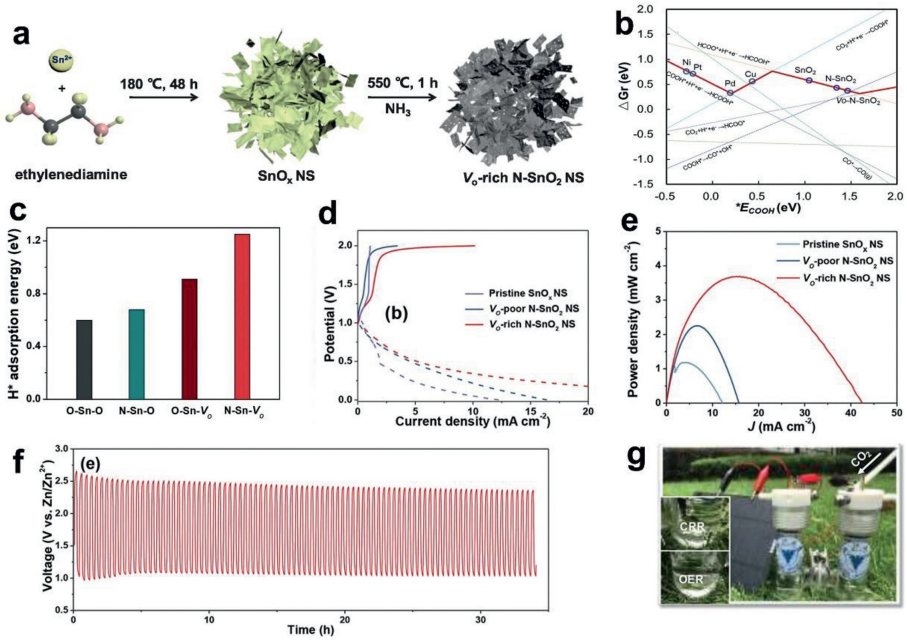

Fig. 9. (a) Structural characterization of the V_O-rich N-SnO_2 NS catalyst. (b) Gibbs free reaction energy as a function of *ECOOH on (211) surface of transition metals and (110) surface of tin-oxides at 298 K without potential correction. (c) H* adsorption energy. (d) Charging (solid line) and discharging (dotted line) curves. (e) Power density curves. (f) Galvanostatic discharge-charge cycling curve of the VO-rich N-SnO_2 NS catalyst at 1.0 mA/cm^2. (g) Photograph of CRR-OER device driven by solar energy. Copied with permission [49]. Copyright 2021, Wiley-VCH.

Metal oxides catalysts: In addition to metal catalyst, a new type of N doped SnO_2 nanosheet with oxygen vacancies (V_O-rich N-SnO_2 NS) was also reported for promoting CO_2 conversion to $HCOO^-$ (Fig. 9a) [49]. Low coordination Sn-N moieties are the active sites with optimal electronic and geometric structures tailored by V_O and N dopants, leading to the reduced reaction free energy of HCOO* protonation over the catalyst (Fig. 9b). HER is also suppressed with N dopant and V_O (Fig. 9c). The corresponding Zn-CO_2 battery shows an open-circuit voltage close to theoretical value of 0.95 V (Fig. 9d). A peak power density of 3.67 mW/cm^2 at 0.23 V is achieved in this battery, along with a formate FE of 74% at 6.0 mA/cm^2 (Fig. 9e). OER is regarded as the anodic reduction during charging process. This battery delivers a charge-discharge voltage difference of 1.47 and 1.66 V at 5 and 10 mA/cm^2, respectively. After a consecutive 100 cycles of 33 h, the Zn-CO_2 battery shows the slightly reduced performance (Fig. 9f) and this battery can be powered by solar energy (Fig. 9g). ZnIn oxide has also been reported as catalyst cathode material in an aqueous rechargeable Zn-CO_2 battery with an open-circuit voltage of 1.35 V and a power density of 1.32 mW/cm^2 [50].

2.2.3. Catalyst cathodes for Zn-CO_2 batteries for CH_4 production

As most Zn-CO_2 batteries focus on the production on CO and $HCOO^-$, which involves only 2 or 3 electrons transfer, CRR to hydrocarbons with kinetically challenging proton-coupled electron transfer process is rarely reported [81]. Only two works about Zn-CO_2 batteries for CH_4 production have been reported based on the ionic liquid electrolyte. Hu *et al.* reported a flow battery with a hollow fiber of carbon nanotubes (CHF) as cathode (Figs. 10a and b), Zn wire as anode, and [EMIM][BF_4] as electrolyte for CH_4 production with a FE up to 94% [53]. Simultaneously, the battery produces electricity, with an energy density of 288.3 Wh/kg (based on the zinc mass) and a stability up to 8 days (Figs. 10c-f). The superior electrochemical performance is ascribed to the availability of protons ensured by the water shuttle between anode and electrolyte. Furthermore, $[EMIM]^+$ in electrolyte plays a crucial role to enhance the adsorption of CO_2 and reduce kinetic barriers. Cao *et al.* report CNTs@Cu to assemble two primary Zn-CO_2 flow batteries 1-ethyl-3-methylimidazolium tetrafluoroborate as electrolyte [54]. The flow battery can convert CO_2 into CH_4 with a FE of 93.3% and supply electricity with an energy density of 376 Wh/kg. This battery remains stable for more than 18 days. These excellent performances are attributed to a synergistic effect involving CNTs and the metal substrate.

3. Zn-N_2 batteries

3.1. Mechanisms

Current Zn-N_2 batteries focus on the production of NH_3 from the N_2 in the aqueous solution. Similar to Zn-CO_2 battery, Zn-N_2 batteries also employs a H-type configuration separated by a bipolar/proton membrane to support the mass transportation while blocking the diffusion of generated ammonia at the cathode. Du *et al.* first reported a primary Zn-N_2 battery for simultaneous NH_3 synthesis and electricity generation as a new application for the N_2 reduction reaction (NRR) [82]. The electrochemical reactions on each electrode are described as follows:

$$\text{Cathode: } N_2 + 6H_2O + 6e^- \rightarrow 2NH_3 + 6OH^-$$

$$\text{Anode: } Zn + 2OH^- \rightarrow ZnO + H_2O + 2e^-$$

$$\text{Overall reaction: } 3Zn + N_2 + 3H_2O \rightarrow 3ZnO + 2NH_3$$

Subsequently, Wang *et al.* assembled a rechargeable aqueous Zn-N_2 battery, in which NRR and OER processes separately occur on the cathode during discharge and charge stages, for sustainable NH_3 production [83]. The reactions at the electrodes during the discharging process are the same with the aforementioned report. For the battery charge process, the reactions can be written as follows:

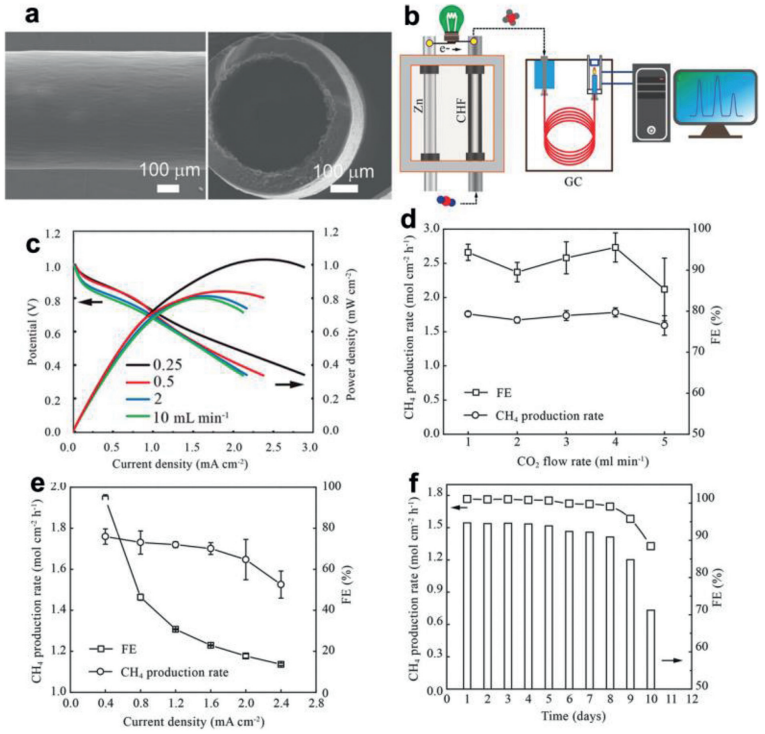

Fig. 10. (a) SEM images of CHF. (b) A schematic structure of the Zn-CO_2 flow battery. (c) Polarization and power density curves of the Zn-CO_2 flow battery at different CO_2 flow rates. (d) Production rates and FEs for CH_4. (e) Production rates and FEs for CH_4 at different current densities. (f) Production rates and FFs for CH_4 over 10 days. Copied with permission [53]. Copyright 2020, Wiley-VCH.

Anode: $4OH^- \rightarrow O_2 + 2H_2O + 4e^-$

Cathode: $ZnO + H_2O + 2e^- \rightarrow Zn + 2OH^-$

The overall reaction of Zn-N_2 battery can be written as: $2N_2 + 6H_2O \rightarrow 4NH_3 + 3O_2$.

3.2. Catalyst cathode in Zn-N_2 batteries for N_2-to-NH_3 conversion

According to the above discussion, it is clear that the production efficiency of NH_3 and the overall battery efficiency of such a rechargeable Zn-N_2 battery depend greatly on the highly efficient bifunctional electrocatalytic performance toward both NRR and OER. HER is a competitive reaction for NRR in aqueous solution due to its very low standard potential of 0 V *vs.* RHE and the high chemical stability and low proton affinity of N_2 molecules [84,85]. The currently reported catalyst cathodes for Zn-N_2 batteries are various, including transition metal and its oxide, phosphates, sulfides, nitride and the hybrids with carbon-based materials.

3.2.1. Transition metal

Metallic Cu was first used in Zn-N_2 battery because Cu has poor HER activity and it is a necessary cofactor for the symbiotic nitrogen fixation process in nitrogenase during legume nodulation [82]. By controlling the monolayer thickness of Cu nanoparticles, the mass transport barrier can be flexibly tailored to finally achieve a high NH_3 FE of 59% in a Zn-N_2 battery with a maximum power density of 10.1 μW/cm^2 in N_2-saturated 0.1 mol/L KOH electrolyte.

3.2.2. Transition metal oxide

Oxygen vacancies (OVs) can donate electrons to antibonding p*-orbitals and thus weaken the triple bond in N_2. Therefore, iron-doped titanium dioxide hollow nanospheres (FeHTNs) with abundant oxygen vacancies was also reported for NRRs [86]. The unique hollow structure and porous shell of FeHTNs provides rich active sites and facilitate the transport of N_2 onto the inner surface of electrolyte. The produced NH_3 induce a negative pressure in cavities, sucking N_2 automatically into the cavity and accelerating the NRR process. The assembled Zn-N_2 aqueous battery shows an average NH_3 yield of 0.172 mg h^{-1} cm^{-2} and a power density: 16.42 mW/cm^2 for energy supply.

3.2.3. Transition metal nitride

Transition metal nitrides (TMNs) have a similar catalytic mechanism to the OVs enriched catalyst and are also regarded as promising catalysts for efficient NRR. Accordingly, Lv *et al.* reported a vanadium nitride nanodots embedded in ultrathin N,S-codoped carbon matrix (denoted as VN@NSC)-based Zn-N_2 cell can deliver a power density of 16.42 μW/cm^2 [87]. However, these three Zn-N_2 cells are primary batteries and the Zn anode is not newable. In addition, no NH_3 FE and the stability were mentioned in this work.

3.2.4. Transition metal sulfide

Two-dimensional (2D) transition metal compounds have shown great potentials in NRR electrocatalysis for ammonia synthesis with unique layered structure [88]. Wang *et al.* fabricated exfoliated metallic niobium disulfate (NbS_2) nanosheets as catalyst cathode for a rechargeable Zn-N_2 battery [83]. Thanks to more exposed active sites and high electron transfer ability of NbS_2, this battery shows a specific capacity of 714 mAh/g with a power density of 0.31 mW/cm^2. Meantime, the Zn-N_2 battery at a settled current density of 0.05 mA/cm^2 for a constant running of 10 h. Wang *et al.* exfoliated $FePS_3$ nanosheet with rich sulfur vacancies

Table 1
Comparison of reported Zn-CO_2 batteries.

Cathode catalysts	Anolyte	Catholyte	Open circuit (V)	Maximum power density (mW/cm^2)	Cathodic products	Maximum FE (%)	Ref.
Coralloid Au	6 mol/L KOH + 0.2 mol/L $Zn(AC)_2$	0.5 mol/L $KHCO_3$	~1.1	0.7	CO	63	[58]
Au@Ir	0.8 mol/L KOH + 0.02 mol/L $Zn(AC)_2$	0.8 mol/L $KHCO_3$	0.803	-	CO	90	[59]
Cu–N_2/GN	6 mol/L KOH + 0.2 mol/L $Zn(AC)_2$	0.5 mol/L $KHCO_3$	~1.8	0.6	CO	64	[45]
Ni-N_3-C	8 mol/L KOH + 0.02 mol/L $Zn(AC)_2$	0.8 mol/L $KHCO_3$	-	-	CO	93	[46]
CA/N-Ni	6 mol/L KOH + 0.2 mol/L $Zn(AC)_2$	0.5 mol/L $KHCO_3$	~0.75	0.5	CO	98	[61]
DNG-SAFe	6 mol/L KOH + 0.2 mol/L $Zn(AC)_2$	1 mol/L $KHCO_3$	~0.86	0.925	CO	86.5	[63]
Ni-N_3-NCNFs	6 mol/L KOH + 0.2 mol/L $Zn(AC)_2$	0.5 mol/L $KHCO_3$	~0.6	1.05	CO	96	[64]
Fe_1NC/S_1-1000	0.8 mol/L KOH + 0.02 mol/L $Zn(AC)_2$	0.8 mol/L $KHCO_3$	0.727	0.75	CO	-	[65]
NiFe-DASC	2 mol/L KOH + 0.02 mol/L $Zn(AC)_2$	2 M KCl	~0.85	1.36	CO	90.6	[66]
Fe_1-Ni_1-N-C	6 mol/L KOH	0.5 mol/L $KHCO_3$	-	-	CO	93.4	[67]
NOMC	6 mol/L KOH + 0.2 mol/L $Zn(AC)_2$	0.8 mol/L $KHCO_3$	~0.5	0.71	CO	76	[70]
NiPG	6 mol/L KOH + 0.2 mol/L $Zn(AC)_2$	3 mol/L $KHCO_3$	-	-	CO	66	[73]
V-$CuInSe_2$	1 mol/L KOH + 0.02 mol/L $Zn(AC)_2$	0.5 mol/L $KHCO_3$	~1	0.75	CO	-	[74]
Cu_3P/C	4 mol/L NaOH	0.1 mol/L $NaHCO_3$	1.5	2.6	CO	-	[75]
ZrO_2@Ni-NC	6 mol/L KOH	0.5 mol/L $KHCO_3$	~0.7	1.5	CO	94.3	[77]
Ni_9Cu_1@NCNTs/CFM	6 mol/L KOH + 0.2 mol/L $Zn(AC)_2$	0.5 mol/L $KHCO_3$	~0.93	0.65	CO	-	[78]
s-SnLi	6 mol/L KOH + 0.2 mol/L $Zn(AC)_2$	6 mol/L KOH + 0.2 mol/L $Zn(AC)_2$	-	1.24	$HCOO^-$	-	[48]
VO-rich N-SnO_2 NS	0.1 mol/L KOH	0.1 mol/L $KHCO_3$	1	3.67	$HCOO^-$	74	[49]
In/ZnO@C	0.8 mol/L KOH + 0.02 mol/L $Zn(AC)_2$	0.8 mol/L $KHCO_3$	1.35	1.32	$HCOO^-$	57	[50]
PNCB	0.2 mol/L KOH + 0.02 mol/L $Zn(AC)_2$	0.2 mol/L $KHCO_3$ + 0.02 mol/L HCOOH	1.1	1.43	$HCOO^-$	80	[51]
Pd IN	1 mol/L KOH + 0.02 mol/L $Zn(AC)_2$	1 mol/L NaCl + 0.1 mol/L NaAc	0.89	-	$HCOO^-$	> 80	[52]
CNF	[EMIM][BF_4] ionic liquid		1.01	0.7999	CH_4	-	[53]
CNTs/Cu	[EMIM][BF_4] ionic liquid		0.82	1.889	CH_4	-	[54]

(Vs-$FePS_3$ NSs) prepared by an efficient electrochemical exfoliation treatment of bulk $FePS_3$ in an organic electrolyte, followed by an annealing treatment in 5% H_2/Ar atmosphere. Attributed to the highly exposed S vacancies which promotes the hydrogenation of N_2 molecules and active Fe sites for N_2 reduction, the Vs-$FePS_3$ NSs equipped rechargeable Zn-N_2 battery delivers a power density of 2.6 mW/cm^2. In addition, the battery delivers a stable voltage during discharging process at 0.05 mA/cm^2 with a specific capacity of 833 mAh/g [89].

3.2.5. Transition metal phosphate

Focusing on constructing a bifunctional catalyst for both OER and NRR at the cathode to make the Zn-N_2 battery a better cycling capability, Ren *et al.* prepared the bifunctional cobalt phosphate nanocrystals-loaded heteroatoms-doped carbon nanosheets (CoPi/NPCS) (Fig. 11a) for a rechargeable Zn-N_2 battery [90]. The NRR mechanism happened on CoPi/NPCS should reasonably follows the associative pathway (Fig. 11b), wherein protons are coupled with N_2 to form N_2H_y intermediates, and finally leaving NH_3. This battery can be powered by a silicon photovoltaic cell (Fig. 11c). A peak power density of 0.49 mW/cm^2 is achieved of this Zn-N_2 battery and the energy density in the discharge process is calculated to be 147.6 mWh/g_{zn} (Figs. 11d and e). During charge process, an enhanced NH_3 yield rate of 14.7 μg h^{-1} $mg_{cat.}^{-1}$ and FE of 16.35% are achieved (Fig. 11f), decreased charge-discharge voltage gaps, and excellent cycling stability over 20 cycles (Figs. 10g and h) [90]. More Co^{3+} are generate at the charging potential (Fig. 11i). These findings not only demonstrate the possibility of different transition metal compounds as bifunctional catalyst cathodes in a rechargeable Zn-N_2 batteries for sustainable NH_3 synthesis from useless N_2 and power generation simultaneously [91].

4. Zn-NO batteries

4.1. Mechanisms

Primary Zn-NO batteries has emerged with the NH_3 synthesis from selective NO reduction. The batteries are performed in a H-type configuration. The catalyst cathodes are placed in a cathodic electrolyte (acidic or neutral solution) and a polished Zn plate is set in an anodic electrolyte (1 mol/L KOH or NaOH), separated by a bipolar membrane. During the battery discharge process, the electrochemical reactions on each electrode can be described as follows [92]:

Cathode: $NO + 5H^+ + 5e^- \rightarrow NH_3 + H_2O$

Anode: $Zn + 2OH^- \rightarrow ZnO + H_2O + 2e^-$

Overall: $5Zn + 2NO + 3H_2O \rightarrow 5ZnO + 2NH_3$

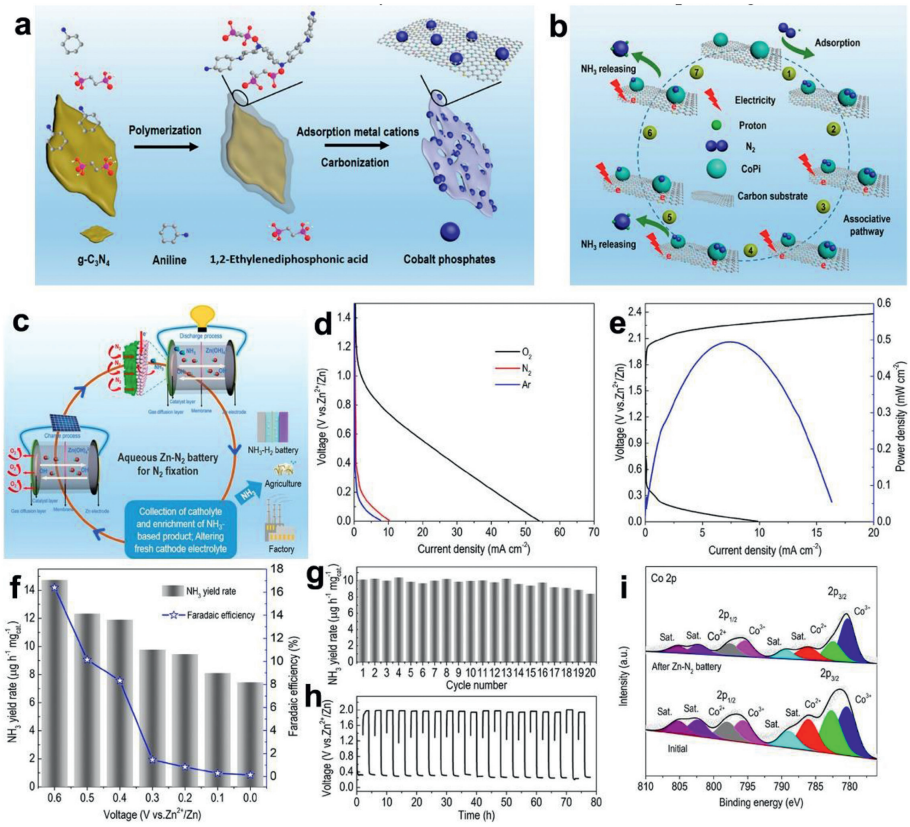

Fig. 11. (a) Schematic illustration of the synthesis of CoPi/NPCS. (b) Possible reaction pathway on CoPi/NPCS for NRR. (c) Schematic illustration of rechargable Zn-N_2 battery. (d) Discharge polarization curves. (e) Charge-discharge polarization curves and corresponding power density. (f) Dependence of the NH_3 yield rate and the FE on the various discharge voltages. (g) NH_3 yield rate under various discharge process of CoPi/NPCS-catalyzed battery. (h) Charge-discharge cycling curves. (i) High-resolution XPS Co 2p spectra of CoPi/NPCS before and after Zn-N_2 battery cycling tests. Copied with permission [90]. Copyright 2021, American Chemical Society.

4.2. Catalyst cathodes for Zn-NO batteries for NH_3 production

NO reduction involves multi-electron transfer process and previous work focus on the conversion of NO to harmless N_2, which however suffers from high operation cost and secondary pollution [93]. Compared to N_2, NO has a higher water solubility and lower bond energy. It is more attractive to convert NO electrochemically to NH_3 in aqueous media and active electrocatalysts is crucial in this process. Nowadays, MoS_2 [92], NiO [94] and Ni_2P [95] have been reported as efficient NO reduction reaction (NORR) catalyst cathode for Zn-NO batteries. MoS_2/CP-based Zn-NO battery (Fig. 12a) delivers a high open-circuit voltage (OCV) of approximately 2.03 V (Fig. 12b) and a high-power density of 1.04 mW/cm^2 at 1 mA/cm^2 (Fig. 12c). This battery achieves a maximal NH_3 yield of 411.8 μg h^{-1} $mg_{cat.}^{-1}$ (Fig. 12d), considerably outperforming most recent metal-N_2 battery systems. The positively charged Mo-edge sites facilitate NO adsorption/activation *via* an acceptance-donation mechanism and disfavor the binding of protons and the coupling of N-N bond (Fig. 12e). Ni_2P equipped Zn-NO battery shows a slightly higher OCV of 2.06 V than MoS_2-based ones, with a discharge power density of 1.53 mW/cm^2 and an NH_3 yield of 62.05 μg h^{-1} $mg_{cat.}^{-1}$. NiO catalyst shows inferior activity compared to MoS_2 and Ni_2P. NO electrochemistry thus offers a new gas-based Zn-based energy conversion/storage device. The catalysis and battery performance of currently reported Zn-gas batteries have been summarized in Tables 1–3 for comparison.

5. Zn-Cl_2 batteries

In addition to the most commonly reported Zn-gas battery, Zn-Cl_2 battery was also reported in the past. Different from CO_2, N_2, and NO conversion to produce value-added chemicals at the cathode with small power density, Cl_2 redox reaction proceeds gas-liquid phase-conversion reactions with high reaction potential as 1.36 V *vs.* RHE (pH 0), and outstanding theoretical gravimetric capacity as 756 mAh/g based on a one-electron Cl-based conversion reaction [96]. However, exploiting Cl-redox electrode was largely stranded within the past 4 decades due to the conspicuous leakage issue of gaseous Cl_2 with safety concerns [97].

6. Conclusion and outlook

Zn-gas batteries have attracted increasing attention in the past few years due to their high potential in energy storage and upcycling of the pollutant or useless gases, including CO_2, N_2 and NO. This review concluded the latest research progress of these Zn-gas batteries. Battery mechanism and cathodic catalyst materials, which play a key role in the battery performance, are comprehensively summarized. This review offers a clear cognition of the future selection of suitable catalysts through comparing their catalytic activity.

However, the development of aforementioned Zn-gas batteries is still in the initial stage, and there are still certain challenges in these fields and further exploration is needed in the future.

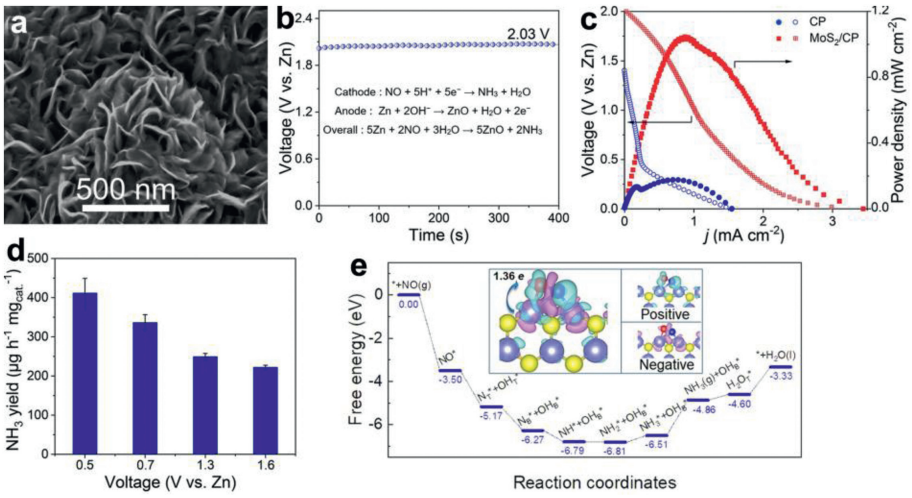

Fig. 12. (a) SEM image of MoS_2 nanosheet. (b) OCV of Zn-NO battery. (c) Polarization and power density curves of the Zn-NO battery. (d) NH_3 yield of Zn-NO battery at different voltages. (e) Free energy landscape for NORR on MoS_2. Copied with permission [91]. Copyright 2021, Wiley-VCH.

Table 2
Comparison of reported Zn-N_2 batteries.

Cathode catalysts	Anolyte	Catholyte	Open circuit (V)	Maximum power density (mW/cm^2)	Ammonia yield	Maximum FE (%)	Ref.
Cu NPs	0.1 mol/L KOH	0.1 mol/L KOH	~0.5	0.0101	1.4 μg h^{-1} cm^{-2}	59	[82]
NbS_2 NS	-	-	~1.3	0.31	-	4.03	[83]
FeHTNs	0.1 mol/L KOH	0.1 mol/L KOH	~0.6	0.02765	0.137 μg h^{-1} cm^{-2}	-	[86]
VN@NSC	0.1 mol/L KOH	0.1 mol/L KOH	~0.55	0.01642	0.172 μg h^{-1} cm^{-2}	~12	[87]
Vs-$FePS_3$ NSs	Alkaline anolyte	0.1 mol/L HCl	~1.75	2.6	-	-	[89]
CoPi/NPCS	1.0 mol/L KOH	1.0 mol/L KOH	~1.4	0.49	14.6 μg h^{-1} mg$_{cat.}^{-1}$	16.35	[90]
CoPi/HSNPC	1 mol/L KOH	1 mol/L KOH	~1	0.31	11.62 μg h^{-1} mg$_{cat.}^{-1}$	24.42	[91]

Table 3
Comparison of reported Zn-NO batteries.

Cathode catalysts	Anolyte	Catholyte	Open circuit (V)	Maximum power density (mW/cm^2)	Ammonia yield	Maximum FE (%)	Ref.
MoS_2/GF	1 mol/L KOH	0.1 mol/L HCl + 0.5 mmol/L Fe(II)SB	2.03	1.04	411.8 mg h^{-1} mg$_{cat.}^{-1}$	4.03	[92]
NiO nanosheet	1 mol/L NaOH	0.1 mol/L Na_2SO_4	1.525	0.88	228 μg h^{-1} cm^{-1}	24.42	[94]
Ni_2P nanoarray	1 mol/L KOH	0.1 mol/L HCl	2.06	1.53	62.05 μg h^{-1} mg$_{cat.}^{-1}$	16.35	[95]

(1) Developing Zn-gas batteries for more various chemicals production

Up to sixteen valuable chemicals can be produced from CO_2 reduction using active catalysts with high selectivity. However, only CO, $HCOO^-$ and CH_4 production are reported *via* Zn-CO_2 batteries. It is suggested to produce more value-added chemicals, such as alcohols and ethylene, from battery systems. It is also highly attractive if hydrazine, a liquid fuel, can be produced from the Zn-N_2/NO batteries. To achieve this aim, intense effort should be devoted to exploring efficient catalyst cathode.

(2) Employment of *operando* techniques to analysis battery performance

Although some *in situ* characterization have been used in electrocatalytic CRR and NRR in a three-electrode system, their application to study the battery performance is rare. The *operando* techniques can analyze the activity and selectivity of catalyst cathodes synchronously, while reaction conditions are close to real working environments. This study shows a clear and accurate insight into the reaction mechanism and formation of different intermediates by *operando* techniques, providing important guidance for designing more efficient catalysts.

(3) Rational catalyst design for improvement of Zn-gas batteries

As the emerging devices of energy storage and chemicals production, many aspects of Zn-gas batteries must still be improved, such as low output voltage, low production rate and FE, inferior durability and low power density for practical applications. For instance, electrolysis of CRR in a flow cell can deliver a current density of 200 mA/cm^2 with a superior CO selectivity of 96.8% at −1.58 V using ZrO_2@Ni-NC catalyst. However, during the discharge process, the cathode ZrO_2@Ni-NC equipped in a Zn-CO_2 battery could only achieve the highest CO FE of 94.3% at a small current of 4.0 mA. In addition, most reported Zn-gas batteries could only cycle no more than 100 h with a high charge voltage up to 3 V and their power density is lower than 10 mW/cm^2, much smaller than ZABs. The improvement of Zn-gas batteries is urgently needed in the future and the bifunctional catalyst with high efficiency for CRR is highly desirable. The same applies to NRR and NORR. Theoretical research *via* machine learning is suggested in the future to assistant the exploration of highly efficient catalyst cathode materials.

(4) Novel design of CRR, NRR and NORR electrolyzer

Traditional H-type setup can only work for tens of hours and exhibit a limited current density of 100 mA/cm^2, which does not meet the industrial production requirement. Thus, the membrane electrode assembly cell, which comprises the gas diffusion electrode and ion-exchange membrane is introduced to solve these problems. Or more efforts are demanded to design more convenient electrochemical cell with fast charge/electron transport.

Declaration of competing interest

We declare that we do not have any commercial or associative interest that represents a conflict of interest in connection with the work submitted.

Acknowledgment

This research was supported by GRF under Project CityU (No. 11212920).

References

[1] N. Armaroli, V. Balzani, Energy Environ. Sci. 4 (2011) 3193–3222.
[2] S. Zhang, D. Chen, Z. Liu, M. Ruan, Z. Guo, Appl. Catal. B: Environ. 284 (2021) 119686.
[3] D. Chen, Z. Liu, S. Zhang, Appl. Catal. B: Environ. 265 (2020) 118580.
[4] C. Smith, A.K. Hill, L. Torrente-Murciano, Energy Environ. Sci. 13 (2020) 331–344.
[5] Y. Hou, J. Wang, C. Hou, et al., J. Mater. Chem. A 7 (2019) 6552–6561.
[6] Y. Hou, J. Wang, J. Liu, et al., Adv. Energy Mater. 9 (2019) 1901751.
[7] Z. Huang, Y. Hou, T. Wang, et al., Nat. Commun. 12 (2021) 3106.
[8] H. Zhang, Y. Yang, D. Ren, L. Wang, X. He, Energy Storage Mater. 36 (2021) 147–170.
[9] Z. Liu, Y. Huang, Y. Huang, et al., Chem. Soc. Rev. 49 (2020) 180–232.
[10] Z. Huang, X. Li, Q. Yang, et al., J. Mater. Chem. A 7 (2019) 18915–18924.
[11] L. Wang, G. Fan, J. Liu, et al., Chin. Chem. Lett. 32 (2021) 1095–1100.
[12] Y. Wang, N. Wu, Y. Qi, et al., App. Sur. Sci. 585 (2022) 152569.
[13] T. Zhang, N. Wu, Y. Zhao, et al., Adv. Sci. 9 (2021) 2103954.
[14] M. Wu, G. Zhang, H. Yang, et al., InfoMat 4 (2021) e12265.
[15] F. Liang, K. Zhang, L. Zhang, et al., Small 17 (2021) 2100323.
[16] S. Zhang, B. Zhang, D. Chen, et al., Nano Energy 79 (2021) 105485.
[17] S. Zhang, Z. Liu, D. Chen, W. Yan, Appl. Catal. B: Environ. 277 (2020) 119197.
[18] B. Zhang, Y. Jiang, M. Gao, et al., Nano Energy 80 (2021) 105504.
[19] H. Yang, X. Wang, Q. Hu, et al., Small Methods 4 (2020) 1900826.
[20] Z. Huang, T. Wang, H. Song, et al., Angew. Chem. Int. Ed. 60 (2021) 1011–1021.
[21] P. Friedlingstein, R.A. Houghton, G. Marland, et al., Nat. Geosci. 3 (2010) 811–812.
[22] D. Chen, Z. Liu, Z. Guo, W. Yan, M. Ruan, Chem. Eng. J. 381 (2020) 122655.
[23] M.A.A. Aziz, A.A. Jalil, S. Triwahyono, A. Ahmad, Green Chem. 17 (2015) 2647–2663.
[24] K. Caldeira, A.K. Jain, M.I. Hoffert, Science 299 (2003) 2052–2054.
[25] F. He, X. Zhu, L. Zhong, Z. Li, Y. Qian, Chin. Chem. Lett. 32 (2021) 3175–3179.
[26] X. Zhang, L. Han, H. Chen, S. Wang, Chin. Chem. Lett. 33 (2021) 1117–1130.
[27] R. Zhang, C. Tang, R. Kong, et al., Nanoscale 9 (2017) 4793–4800.
[28] R. Zhang, X. Ren, X. Shi, et al., ACS Appl. Mater. Interfaces 10 (2018) 28251–28255.
[29] Y. Guo, J. Gu, R. Zhang, et al., Adv. Energy Mater. 11 (2021) 2101699.
[30] Y. Guo, J. Liu, Q. Yang, et al., Nano Energy 86 (2021) 106099.
[31] H.A. Hansen, J.B. Varley, A.A. Peterson, J.K. Nørskov, J. Phys. Chem. Lett. 4 (2013) 388–392.
[32] Z. Chen, G. Zhang, L. Du, et al., Small 16 (2020) 2004158.
[33] Y. Zhang, L. Ji, W. Qiu, et al., Chem. Commun. 54 (2018) 2666–2669.
[34] A. Vasileff, Y. Zheng, S.Z. Qiao, Adv. Energy Mater. 7 (2017) 1700759.
[35] X. Lu, D.Y.C. Leung, H. Wang, M.K.H. Leung, J. Xuan, ChemElectroChem 1 (2014) 836–849.
[36] L. Li, C. Tang, H. Jin, K. Davey, S.Z. Qiao, Chem 7 (2021) 3232–3255.
[37] G. Soloveichik, Nat. Catal. 2 (2019) 377–380.
[38] Y. Guo, Q. Yang, D. Wang, et al., Energy Environ. Sci. 13 (2020) 2888–2895.
[39] R. Zhang, Y. Zhang, X. Ren, et al., ACS Sustain. Chem. Eng. 6 (2018) 9545–9549.
[40] Y. Guo, R. Zhang, S. Zhang, et al., Energy Environ. Sci. 14 (2021) 3938–3944.
[41] R. Zhang, Y. Guo, S. Zhang, et al., Adv. Energy Mater. 12 (2022) 2103872.
[42] J. Xie, Y. Wang, Acc. Chem. Res. 52 (2019) 1721–1729.
[43] Z. Huang, T. Wang, X. Li, et al., Adv. Mater. 34 (2021) 2106180.
[44] Z. Huang, A. Chen, F. Mo, et al., Adv. Energy Mater. 10 (2020) 2001024.
[45] W. Zheng, J. Yang, H. Chen, et al., Adv. Funct. Mater. 30 (2020) 1907658.
[46] Y. Zhang, L. Jiao, W. Yang, C. Xie, H.L. Jiang, Angew. Chem. Int. Ed. 60 (2021) 7607–7611.
[47] A. Del Castillo, M. Alvarez-Guerra, J. Solla-Gullón, et al., J. CO_2 Util. 18 (2017) 222–228.
[48] S. Yan, C. Peng, C. Yang, et al., Angew. Chem. Int. Ed. 60 (2021) 25741–25745.
[49] Z. Li, A. Cao, Q. Zheng, et al., Adv. Mater. 33 (2021) 2005113.
[50] X. Teng, Y. Niu, S. Gong, et al., Mater. Chem. Front. 5 (2021) 6618–6627.
[51] Y. Wang, L. Xu, L. Zhan, et al., Nano Energy 92 (2022) 106780.
[52] J. Xie, X. Wang, J. Lv, et al., Angew. Chem. Int. Ed. 57 (2018) 16996–17001.
[53] K. Wang, Y. Wu, X. Cao, L. Gu, J. Hu, Adv. Funct. Mater. 30 (2020) 1908965.
[54] Y. Chen, Y. Mei, M. Li, et al., Green Chem. 23 (2021) 8138–8146.
[55] X.M. Hu, H.H. Hval, E.T. Bjerglund, et al., ACS Catal. 8 (2018) 6255–6264.
[56] Y. Zhang, X.Y. Zhang, K. Chen, W.Y. Sun, ChemSusChem 14 (2021) 1847–1852.
[57] Y. Chen, C.W. Li, M.W. Kanan, J. Am. Chem. Soc. 134 (2012) 19969–19972.
[58] S. Gao, M. Jin, J. Sun, et al., J. Mater. Chem. A 9 (2021) 21024–21031.
[59] X. Wang, J. Xie, M.A. Ghausi, et al., Adv. Mater. 31 (2019) 1807807.
[60] Z. Zeng, A.G.A. Mohamed, X. Zhang, Y. Wang, Energy Technol. 9 (2021) 2100205.
[61] Y. Zhang, X. Wang, S. Zheng, et al., Adv. Funct. Mater. 31 (2021) 2104377.
[62] J. Chen, Z. Li, X. Wang, et al., Angew. Chem. Int. Ed. 61 (2021) e202111.
[63] W. Ni, Z. Liu, Y. Zhang, et al., Adv. Mater. 33 (2021) 2003238.
[64] W. Zheng, Y. Wang, L. Shuai, et al., Adv. Funct. Mater. 31 (2021) 2008146.
[65] T. Wang, X. Sang, W. Zheng, et al., Adv. Mater. 32 (2020) 2002430.
[66] Z. Zeng, L.Y. Gan, H.Bin Yang, et al., Nat. Commun. 12 (2021) 4088.
[67] L. Jiao, J. Zhu, Y. Zhang, et al., J. Am. Chem. Soc. 143 (2021) 19417–19424.
[68] P. Li, H. Li, D. Han, et al., Adv. Sci. 6 (2019) 1802355.
[69] P. Li, T. Shang, X. Dong, et al., Small (2021) 2007548.
[70] S. Gao, Y. Liu, Z. Xie, et al., Small Methods 5 (2021) 2001039.
[71] X. Hao, X. An, A.M. Patil, et al., ACS Appl. Mater. Interfaces 13 (2021) 3738–3747.
[72] X. Wang, M.A. Ghausi, R. Yang, et al., J. Mater. Chem. A 8 (2020) 13806–13811.
[73] R. Yang, J. Xie, Q. Liu, et al., J. Mater. Chem. A 7 (2019) 2575–2580.
[74] J. Wang, X. Zheng, G. Wang, et al., Adv. Mater. 33 (2021) 2106354.
[75] M. Peng, S. Ci, P. Shao, P. Cai, Z. Wen, J. Nanosci. Nanotechnol. 19 (2019) 3232–3236.
[76] X. Liu, S. Tao, J. Zhang, et al., J. Mater. Chem. A 9 (2021) 26061–26068.
[77] X. Wang, S. Feng, W. Lu, et al., Adv. Funct. Mater. 31 (2021) 2104243.
[78] S. Shen, C. Han, B. Wang, Y. Wang, Chin. Chem. Lett. 33 (2022) 3721–3725.
[79] A. Mustafa, Y. Shuai, B.G. Lougou, et al., Chem. Eng. Sci. 245 (2021) 116869.
[80] D. Wu, R. Feng, C. Xu, et al., Nano-Micro Lett. 14 (2022) 38.
[81] M.D. Garba, M. Usman, S. Khan, et al., J. Environ. Chem. Eng. 9 (2021) 104756.
[82] C. Du, Y. Gao, J. Wang, W. Chen, Chem. Commun. 55 (2019) 12801–12804.
[83] H. Wang, J. Si, T. Zhang, et al., Appl. Catal. B: Environ. 270 (2020) 118892.
[84] L. Hollevoet, F. Jardali, Y. Gorbanev, et al., Angew. Chem. Int. Ed. 59 (2021) 23825–23829.
[85] Y. Zhang, W. Qiu, Y. Ma, et al., ACS Catal. 8 (2018) 8540–8544.
[86] X.W. Lv, X.L. Liu, L.J. Gao, J. Mater. Chem. A 9 (2021) 4026–4035.
[87] X.W. Lv, Y. Liu, Y.S. Wang, X.L. Liu, Z.Y. Yuan, Appl. Catal. B: Environ. 280 (2021) 119434.
[88] J. Sun, W. Kong, Z. Jin, et al., Chin. Chem. Lett. 31 (2020) 953–960.
[89] H. Wang, Z. Li, Y. Li, et al., Nano Energy 81 (2021) 105613.
[90] J.T. Ren, L. Chen, H.Y. Wang, Z.Y. Yuan, ACS Appl. Mater. Interfaces 13 (2021) 12106–12117.
[91] J.T. Ren, L. Chen, Y. Liu, Z.Y. Yuan, J. Mater. Chem. A 9 (2021) 11370–11380.
[92] L. Zhang, J. Liang, Y. Wang, et al., Angew. Chem. Int. Ed. 60 (2021) 25263–25268.
[93] L. Han, S. Cai, M. Gao, et al., Chem. Rev. 119 (2019) 10916–10976.
[94] P. Liu, J. Liang, J. Wang, et al., Chem. Commun. 57 (2021) 13562–13565.
[95] T. Mou, J. Liang, Z. Ma, et al., J. Mater. Chem. A 9 (2021) 24268–24275.
[96] G. Liang, F. Mo, X. Ji, C. Zhi, Nat. Rev. Mater. 6 (2021) 109–123.
[97] C. Amato, Report 22 No. 0148-7191, SAE Technical Paper, 1973.